

Computational Model for Transport in Nanotube-Based Composites With Applications to Flexible Electronics

Satish Kumar

School of Mechanical Engineering,
Purdue University,
West Lafayette, IN 47907

Muhammad A. Alam

School of Electrical and Computer Engineering,
Purdue University,
West Lafayette, IN 47907

Jayathi Y. Murthy¹

School of Mechanical Engineering,
Purdue University,
585 Purdue Mall,
West Lafayette, IN 47907
e-mail: jmurthy@ecn.purdue.edu

Thermal and electrical transport in a new class of nanocomposites composed of random isotropic two-dimensional ensembles of nanotubes or nanowires in a substrate (host matrix) is considered for use in the channel region of thin-film transistors (TFTs). The random ensemble of nanotubes is generated numerically and each nanotube is discretized using a finite volume scheme. To simulate transport in composites, the network is embedded in a background substrate mesh, which is also discretized using a finite volume scheme. Energy and charge exchange between nanotubes at the points of contact and between the network and the substrate are accounted for. A variety of test problems are computed for both network transport in the absence of a substrate, as well as for determination of lateral thermal and electrical conductivity in composites. For nanotube networks in the absence of a substrate, the conductance exponent relating the network conductance to the channel length is computed and found to match experimental electrical measurements. The effective thermal conductivity of a nanotube network embedded in a thin substrate is computed for a range of substrate-to-tube conductivity ratios. It is observed that the effective thermal conductivity of the composite saturates to a size-independent value for large enough samples, establishing the limits beyond which bulk behavior obtains. The effective electrical conductivity of carbon nanotube-organic thin films used in organic TFTs is computed and is observed to be in good agreement with the experimental results.

[DOI: 10.1115/1.2709969]

Keywords: nanotube, thin film transistor, nanocomposite, percolation

Introduction

In recent years, there has been growing interest in low-cost large-area manufacture of thin-film transistors (TFTs) on flexible substrates for use in applications such as displays, *e*-paper, *e*-clothing, biological and chemical sensing, conformal radar, and others. TFTs based on amorphous silicon (*a*-Si) now dominate the market for large-area flat-panel displays [1,2]. When transistor performance is not critical, low-cost organic TFTs on flexible, lightweight, plastic substrates [3–7] are emerging as an alternative in many nondisplay applications. For high-performance applications, however, the choices are limited: single crystal silicon or poly-silicon based TFTs [8,9] cannot be manufactured at low temperature (<200°C) and are therefore not suitable for plastic substrates. As a result, researchers are exploring a new class of nanocomposite TFTs based on networks of silicon nanowires (Si-NWs) or carbon nanotubes (CNTs) [10–12]. Here, high-quality, nearly crystalline NWs and CNTs are grown at high temperature on a temporary substrate and released into a carrier fluid, which is then spin coated onto arbitrary (flexible) substrates at room temperature to form a thin film of randomly oriented NWs or CNTs. Once the source and drain contacts are defined, this thin film of nearly crystalline nanowires or nanotubes constitutes the high performance channel of a TFT (see Fig. 1). In other applications, the performance of organic TFTs is improved by dispersing nanotubes at low densities in organic substrates [13]. Since the thermal con-

ductivity of both plastic and organic substrates is very low (~0.1–1 W/mK), and since cooling options are limited if the electronics are to be kept flexible, self-heating is expected to emerge as a significant bottleneck to performance in this new class of electronics. At the same time, the electrical performance of these network composite transistors is poorly understood, and it has been difficult to interpret seemingly disparate experimental data [11,12,14].

An important property determining device performance is the lateral thermal and electrical conductivity of the composite film. The thermal and electrical conductivity of the network composite depends on the percolation properties of the network. In the absence of the substrate, the network conductivity is zero if the tube density is below the percolation threshold [15]. The presence of the substrate allows conduction to occur below the percolation threshold, and the degree to which percolation matters depends in large part on the coherence length of transport in the tubes [16], i.e., the length over which the temperatures of the two media remain unequilibrated. In the limit of low coherence length, leakage of either heat or charge from the tubes to the substrate predominates, and percolation effects are unimportant. On the other hand, if the coherence length is competitive with the sample size, network percolation would be important. The thermal and electrical behavior of TFTs spans these limits. In general, both substrate and network play important roles in determining the thermal performance of typical nanotube–plastic composites. An analogous problem occurs in electrical transport in nanotube–organic composites whereby charge transport in the organic substrate is enhanced by the presence of subpercolating nanotubes [13]. On the

¹Corresponding author.

Contributed by the Heat Transfer Division of ASME for publication in the JOURNAL OF HEAT TRANSFER. Manuscript received March 28, 2006; final manuscript received August 25, 2006. Review conducted by Sumanta Acharya.

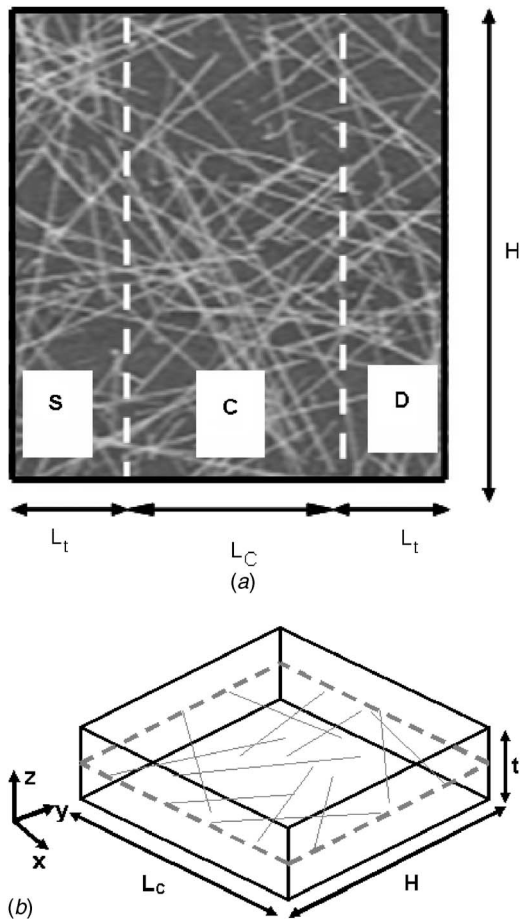


Fig. 1 (a) Schematic of thin-film transistor showing source (S), drain (D), and channel (C). The channel region is composed of a network of CNTs; (b) geometric parameters.

other hand, the electrical conductivity of carbon nanotubes and silicon nanowires in plastic is entirely network dominated due to the nearly insulating substrate.

Though there is much literature on composite thermal and electrical properties [17–19], as well as on the percolation behavior of tubes and wires [14,16,20], two important features distinguish TFT composites. First, our interest is in *finite* nanocomposites, where the length scale of the composite, i.e., the distance between the transistor's source and drain, may be competitive with the length of the nanotubes in the composite, making standard periodic-domain percolation analyses invalid [15]. Second, the composite is a thin film with a thickness of no more than a few microns at the maximum. There are few experimental results or theoretical and computational models which predict the conductivity of finite two-dimensional (2D) nanotube composites. Nearly all experiments have concentrated on bulk 3D samples. Biercuk et al. reported 125% increase in thermal conductivity of epoxy–single wall nanotube (SWNT) composites for 1 wt % SWNT loading at room temperature [21]. Liu et al. used a silicon elastomer as the matrix and CNT as the filler in their experiments and reported 65% enhancement in thermal conductivity with 3.8 wt % CNT loading [22]. Theoretical analyses of bulk composites have, for the most part, addressed low volume fractions using effective medium theories [19], most recently accounting for interfacial resistance [17,23]. However, these studies assume tube densities well below the percolation threshold. Lusti and Gusev predicted the thermoelastic properties of nanotube-reinforced polymers using the finite element method [24]. Using their numerical model, they explored the enhancement in Young's modulus and the de-

crease in thermal expansion coefficient for different orientations of CNTs inside the polymer. Yang and Chen used the phonon Boltzmann equation to study the phonon thermal conductivity of Si–Ge composites using a periodic two-dimensional model [18] and found phonon ballistic effects to be important. However, their findings are appropriate only for aligned rods, with the primary direction for transport being *normal* to the rod axis. To our knowledge, there have been no published analyses of either thermal or electrical transport in nanocomposites composed of random nanotube networks.

The objective of the present work is to develop a framework for the simulation of thermal and electrical transport for finite-length two-dimensional network composites and to validate the model with experimental data where possible. Though our ultimate goal is to simulate the concurrent electro-thermal performance of network TFTs, this paper focuses on the determination of lateral composite conductivity. Thermal transport in the Fourier conduction limit and charge transport in the low bias voltage limit are analogous and can be described by similar governing equations. A random two-dimensional network of tubes is generated numerically and embedded in a substrate. A finite volume method is developed for the coupled solution of the network and the substrate and shown to work satisfactorily by comparison to analytical solutions. The method is then applied to the problem of lateral conductivity determination in 2D networks and composites and shown to match experimental data satisfactorily.

Governing Equations

Thermal Transport. The computational domain is shown in Fig. 1, and is of height H and width L_C . It consists of the channel region of the transistor and is composed of a random network of nanotubes or nanowires embedded in the midplane of a substrate represented by a three-dimensional box of size $L_C \times H \times t$. Diffusive transport in the tube or wire is obtained when there are a sufficient number of scattering events during the residence time of the phonon in the domain. The phonon residence time τ_f scales as L_f/v_g , where v_g is the phonon group velocity. The main scattering events of importance at room temperature in pure samples are either three-phonon processes, occurring on a time scale τ_{3ph} , or boundary scattering events, occurring on a time scale τ_b . For nanowires, $\tau_b \sim d/v_g$, so that $\tau_f/\tau_b \sim L_f/d$; since $L_f/d \gg 1$, diffusive transport due to boundary scattering is expected to prevail. For nanotubes embedded in a substrate, boundary scattering and three-phonon time scales are difficult to estimate and would depend on the nature of the nanotube–substrate interface as well as the modulation of phonon velocities due to the presence of the substrate. However, for sufficiently long tubes, three-phonon processes are expected to lead to diffusive behavior in their own right. For freestanding CNTs, acoustic phonon velocities of 9–20 km/s have been reported in Ref. [25]. Assuming axial thermal conductivities in the 1000 W/mK range, $L/(\tau_{3ph}v_g) \gg 1$ would be achieved for tubes of about 1 μm or longer; the presence of interface scattering is expected to further reduce this value. Thus, Fourier conduction in both nanotubes and nanowires may be assumed, albeit with a thermal conductivity that may differ significantly from bulk or freestanding values. Assuming one-dimensional diffusive transport along the length s of the tube and three-dimensional conduction in the substrate, the governing energy equations in the tube and substrate may be written, respectively, as

$$k_t A \frac{d^2 T_i}{ds^2} + \sum_{\text{intersecting tubes } j} h_c P_c (T_j - T_i) + h_s P_s (T_s - T_i) = 0 \quad (1a)$$

$$k_s \nabla^2 T_s + \sum_{i=1}^{N_{\text{tubes}}} h_s \alpha_v (T_i - T_s) = 0 \quad (1b)$$

Here, $T_i(s)$ is the temperature of the i th tube at a location s along its length; A is the area of cross section of the tube or wire; and k_t is the corresponding thermal conductivity. The term h_c is the heat transfer coefficient governing the transfer of heat to other tubes j making contact with tube i through a contact perimeter P_c , and the heat transfer coefficient h_s governs the transfer of heat between the tube and the substrate through a contact perimeter P_s . $T_s(x, y, z)$ is the substrate temperature and k_s is the substrate thermal conductivity; the second term in Eq. (1b) contains the heat exchange with tubes traversing the substrate, which are N_{tubes} in number, through a contact area per unit volume, α_v . Using the dimensionless variable $\theta = (T - T_{\text{drain}}) / (T_{\text{source}} - T_{\text{drain}})$ and nondimensionalizing all lengths by the tube diameter d , the dimensionless governing equations in the tubes and substrate may be written as

$$\frac{d^2 \theta_i}{ds^{*2}} + \sum_{\text{intersecting tubes } j} Bi_c (\theta_j - \theta_i) + Bi_s (\theta_s - \theta_i) = 0 \quad (2a)$$

$$\nabla^{*2} \theta_s + \sum_{i=1}^{N_{\text{tubes}}} Bi_s \beta_v \frac{k_t}{k_s} (\theta_i - \theta_s) = 0 \quad (2b)$$

For thermal conductivity calculations, the thermal boundary conditions for all tubes originating at the source and terminating in the drain are given by

$$\theta_i = 1 \text{ at } s^* = 0; \quad \theta_i = 0 \text{ at } s^* = \frac{L_t}{d} \quad (3)$$

and the boundary conditions for the substrate are given by

$$\theta_s = 1 \text{ at } x^* = 0; \quad \theta_s = 0 \text{ at } x^* = \frac{L_C}{d}$$

$$\frac{\partial \theta_s}{\partial z^*} = 0 \text{ and at } z^* = 0 \text{ at } z^* = \frac{t}{d} \quad (4)$$

All the tube tips terminating inside the substrate are assumed adiabatic. The boundaries $y^* = 0$ and $y^* = H/d$ are assumed as periodic boundaries for both substrate and tubes. The dimensionless parameters are defined as

$$Bi_c = \frac{h_c P_c d^2}{k_t A}; \quad Bi_s = \frac{h_s P_s d^2}{k_t A}; \quad \frac{k_s}{k_t}$$

$$\beta_v = \alpha_v \left(\frac{A}{P_s} \right); \quad \frac{L_C}{L_t}; \quad \frac{H}{L_t}; \quad \frac{L_t}{d}; \quad \frac{t}{d}$$

Bi_c represents the dimensionless contact conductance for tube-to-tube contact; and Bi_s represents the dimensionless interfacial (Kapitza) resistance between the tube and substrate [17]. The geometric parameter β_v may be determined from the tube density per unit area ρ ; the corresponding dimensionless parameter is ρ^* , which is obtained by normalizing with the percolation threshold ρ_{th} . The percolation threshold for the network is estimated as the density at which the average distance between the nanotubes equals the average length of the tubes, so that $\rho_{\text{th}} = 1 / \langle L_t \rangle^2$.

Electrical Transport. The dimensionless potential equation in the linear regime is analogous to the thermal transport equation in the Fourier conduction limit, with the potential being analogous to temperature and the current being analogous to the heat transfer rate. For charge transport in CNTs in plastic, the substrate is considered insulating and only transport in the tube network is considered. For organic transistors with dispersed CNTs [13], the substrate is not insulating and charge leaks from the CNTs to the organic matrix, analogous to thermal transport in a composite, and

charge exchange with the substrate must be considered. Since $L_C \gg \lambda$, the mean free path of electrons, a drift-diffusion model based on Kirchoff's law for carrier transport may be employed [26]. In this linear regime, which occurs for low source-drain voltage V_{DS} , the current density along the tube is given by

$$J = \sigma d\Phi/ds \quad (5)$$

where σ is the electrical conductivity and Φ is the potential, and is only a function of the source-drain voltage V_{DS} . Using the current continuity equation $dJ/ds = 0$ and accounting for charge transfer to intersecting tubes as well as to the substrate [26], the dimensionless potential distribution ϕ_i along tube i , as well the three-dimensional potential field in the substrate are given by:

$$\frac{d^2 \phi_i}{ds^{*2}} + \sum_{\text{intersecting tubes } j} c_{ij} (\phi_j - \phi_i) + d_{is} (\phi_s - \phi_i) = 0 \quad (6a)$$

$$\nabla^{*2} \phi_s + \sum_{i=1}^{N_{\text{tubes}}} d_{is} \beta_v \frac{\sigma_t}{\sigma_s} (\phi_i - \phi_s) = 0 \quad (6b)$$

Here c_{ij} is the dimensionless charge-transfer coefficient between tubes i and j at their intersection point, analogous to Bi_c in Eq. (2a), and is specified *a priori*; it is nonzero only at the point of intersection. The term d_{is} is analogous to Bi_s term in Eq. (2a) and is active only for nanotubes in organic substrates. The electrical conductivity ratio is σ_t / σ_s . For computing the voltage distribution, boundary conditions $\phi_i = 1.0$ and $\phi_i = 0$ are applied to tube tips embedded in the source and drain regions, respectively. For the organic substrate, $\phi_s = 1.0$ and $\phi_s = 0$ are applied at $x^* = 0$ and $x^* = L_C/d$, respectively; for the other boundaries, a treatment similar to that for the substrate temperature is applied. This computation of voltage distribution is only valid for low V_{DS} . For higher V_{DS} , the complete drift-diffusion equations for electron (n) and hole (p) transport in the network, coupled to a 3D Poisson equation for the potential, would need to be solved [27] and the direct analogy with thermal transport would no longer be valid.

Numerical Method

Network Generation Procedure. We consider a percolating random network of nanotubes or nanowires of length L_t and diameter d randomly dispersed in the midplane of a substrate of thickness t . Thus the nanotube network is essentially 2D, while the substrate containing it is 3D, as shown in Fig. 1(b); the geometry in the midplane is shown in Fig. 1(a). The boundaries at $y^* = 0$ and $y^* = H/d$ are assumed periodic.

The source, drain, and channel regions in Fig. 1 are divided into finite rectangular control volumes. A fixed probability p of a control volume originating a nanotube is chosen a priori. A random number is picked from a uniform distribution and compared with p . If it is less than p , a nanotube is originated from the control volume. The length of source and drain for tube generation is L_t , which ensures that any tube that can penetrate the channel region from either the left or the right is included in the simulations. The orientation of the tube is also chosen from a uniform random number generator. Since the tube length is fixed at L_t , all tubes may not span the channel region even for shorter channel lengths L_C , depending on orientation. Tubes crossing the $y^* = 0$ and $y^* = H/d$ boundaries are treated assuming translational periodicity; that part of the tube crossing one of these boundaries reappears on the other side. Tube-tube intersections are computed from this numerically generated random network and stored for future use. The analysis is conducted only on the tubes that lie in the channel region.

Finite Volume Discretization. We now describe the finite volume discretization procedure [28] used to obtain the temperature distribution in the tubes and the substrate. A similar procedure is adopted for solving the potential equation (Eq. (6)). Each tube is

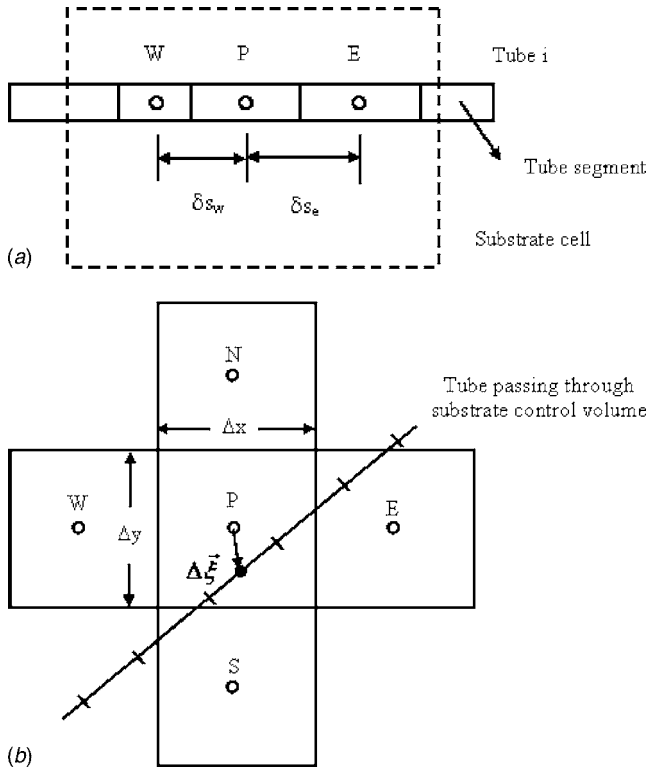


Fig. 2 (a) Tube segment nomenclature, and (b) substrate control volume nomenclature. The displacement vector $\Delta\vec{\xi}$ from substrate cell centroid to tube segment centroid is shown.

divided into 1D segments, as shown in Fig. 2(a) and a control volume balance is performed on each tube segment. Using second-order accurate linear profile assumptions, this yields the following equation for the tube segment i

$$k_t A \frac{T_{E,i} - T_{P,i}}{\delta s_e} - k_t A \frac{T_{P,i} - T_{W,i}}{\delta s_w} + \sum_{\text{intersecting tubes } j} h_c A_c (T_{P,j} - T_{P,i}) + h_s A_s (T'_s - T_{P,i}) = 0 \quad (7)$$

Here, δs_e and δs_w are the distances shown in Fig. 2(a); A_c is the contact area between tubes i and j ; $T_{P,i}$ is the temperature at the control volume P for tube i ; and $T_{P,j}$ is the temperature of intersecting tube j at the same location. Similar conservation equations are written for all the tubes in the domain. Energy lost by tube i to tube j is gained by tube j and vice versa, guaranteeing perfect energy conservation. A_s is the surface area of contact between the tube segment and the substrate, and T'_s is the temperature of the substrate at the location of the cell centroid of tube segment P .

The substrate is discretized into rectangular control volumes of extent $\Delta x \Delta y \Delta z$. Figure 2(b) shows the geometry in 2D for clarity. Writing a control volume balance over each substrate control volume and discretizing using linear profile assumptions, we obtain

$$\sum_{f=1}^6 k_s A_f \frac{T_{nb,s} - T_{P,s}}{\Delta x_f} - \sum_{\text{segments}} h_s A'_{si} (T'_s - T_{P,i}) = 0 \quad (8)$$

Here, $T_{P,s}$ is the substrate temperature at the centroid of the substrate cell P ; f refers to the six faces of cell P ; and A_f to the corresponding face areas. The length Δx_f is distance between the two cell centroids on either side of the face f (between P and E , for example) and $T_{nb,s}$ is the substrate temperature at the neighbor cell centroid (E or W , for example). The summation term represents the heat exchange with all tube segments intersecting the substrate control volume, and A'_{si} is that portion of the tube seg-

ment surface area that is ascribed to substrate cell P . In this way, energy lost by the tube is gained by the substrate and vice versa, and perfect conservation is guaranteed.

Since the substrate discretization is coarser than the tube discretization, it is important to account for gradients in the substrate temperature in determining the term T'_s in the tube–substrate heat exchange in Eqs. (7) and (8). Otherwise, significant errors were found in the calculation, including an inability to reproduce linear temperature profiles exactly in 1D conduction problems with identical tube and substrate thermal conductivities. Therefore, the substrate temperature gradient in the plane of the nanotube network is computed and is used to interpolate the substrate temperature to the tube centroid location

$$T'_s = \nabla T_{P,s} \cdot \Delta\vec{\xi} + T_{P,s} \quad (9)$$

Here $\Delta\vec{\xi}$ is the position vector of tube segment centroid relative to the cell centroid of the substrate, as shown in Fig. 2(b). The substrate temperature gradient in cell P , $\nabla T_{P,s}$, is computed using second-order central difference operators.

Equations (7) and (8) constitute a coupled equation set for the tube segment temperatures T_i and the substrate temperatures T_s at the substrate cell centroids. Though these equations may be solved for each tube and the substrate sequentially and iteratively [28], such a loosely coupled procedure fails when the coupling terms $B_{i,c}$ and $B_{i,s}$ become large. Similar problems occur for long channel lengths and high tube densities; here the equations become strongly coupled to each other due to a large number of tube–tube contacts and a large tube–substrate contact area. Consequently, a direct sparse solver developed by Kundert [29] is used to solve the resulting system of equations. To account for randomness in the sample, most of the results reported here are computed by taking an average over 100 random realizations of the network. More realizations are used for low densities and short channel lengths where statistical invariance is more difficult to obtain due to the small number of tubes in the domain.

Computation of Effective Lateral Thermal Conductivity.

The lateral thermal conductivity of the composite is computed using the expression

$$k_{\text{eff}} = \frac{\sum_{\text{tubes}} k_t A \left. \frac{dT_i}{ds} \right|_{x=0} + \sum_{\text{substrate}} k_s \Delta y \Delta z \left. \frac{dT_s}{dx} \right|_{x=0}}{Ht \left(\frac{T_{\text{drain}} - T_{\text{source}}}{L_c} \right)} \quad (10)$$

where the first term in the numerator is the heat flow through the tubes in the lateral direction, while the second term represents the lateral heat flow in the substrate. The heat flow in both tubes and substrate is computed at the source–channel junction, $x=0$.

Results

In this section, we apply the method described in previous sections to five problems. The first two problems compare numerical results with analytical solutions. The last three problems address lateral conductivity calculations in finite-length nanotube networks and composites both above and below the percolation threshold.

Comparison With Analytical Solution. For the simple case of a CNT composite in which a single CNT is located along the axis of a cylindrically shaped substrate, the temperature distribution in both CNT and substrate can be obtained analytically in the presence of the heat source term inside the CNT. The two ends of the CNT as well as the two planar ends of the substrate cylinder are held at a temperature T_{inf} ; the outer cylindrical surface of the substrate is insulated; and q''' is the average power dissipated per unit volume in the CNT (see inset in Fig. 3). An extra term for Joule heating is added in the Fourier conduction equation for the

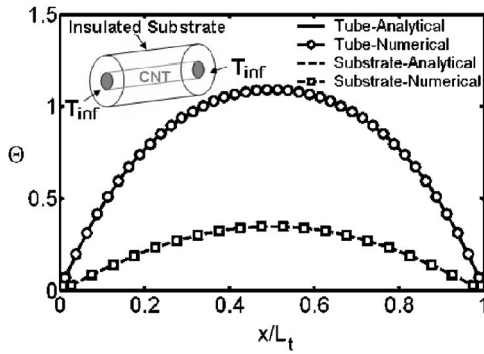


Fig. 3 Comparison of numerically computed dimensionless temperature distribution in tube and substrate with analytical results (θ definition corresponds to that in Eq. (11)). The schematic of the tube embedded in the substrate and the boundary conditions are shown in the inset.

tube [Eq. (2a)]. The temperature distribution inside the tube, T_t , and the substrate, T_s , can be obtained analytically as

$$\theta_t = (T_t - T_{\text{inf}})/(q''L_t^2/k_t) = ae^{\sqrt{c}x} + be^{-\sqrt{c}x} + d(x - x^2) + g \quad (11a)$$

$$\theta_s = (T_s - T_{\text{inf}})/(q''L_t^2/k_t) = [0.5(x - x^2) - \theta_t]/m \quad (11b)$$

where

$$a = \frac{g(e^{\sqrt{c}} - 1)}{(e^{\sqrt{c}} - e^{-\sqrt{c}})}; \quad b = \frac{g(1 - e^{\sqrt{c}})}{(e^{\sqrt{c}} - e^{-\sqrt{c}})}; \quad d = \frac{f}{c}; \quad g = \frac{1 - 2f/c}{c}$$

$$f = \frac{h_s L_t}{2k_t m}; \quad c = \frac{h_s L_t (1 + m)}{k_t m}; \quad m = \frac{k_s}{k_t}$$

The model developed here is used to compute the temperature distribution inside the tube and the substrate and compared against the analytical results. Figure 3 shows a comparison of the computed tube and substrate temperatures for a mesh of 80 tube segments and 20 substrate cells. The numerical results are in excellent agreement with analytical results.

Transport in the Limit of Zero Contact. In the limit when there is no contact between tubes ($Bi_c=0$, $c_{ij}=0$) and between tube and substrate ($Bi_s=0$, $d_{is}=0$) a simple analytical solution for the heat transfer rate through the domain (and correspondingly the drain current I_D for electron transport) may be derived. Only the tubes are considered in this 2D planar calculation, and the substrate contribution is neglected. In this limit, the in-plane heat transfer rate through the composite, q , is directly proportional to the number of bridging tubes N_S (tubes directly bridging source and drain) but inversely proportional to the tube length contained in the channel. By computing the number of bridging tubes from geometric considerations, it may be shown that [26]

$$q \propto I_D \propto \frac{N_S}{W} = \left(\frac{2}{\pi}\right) \rho H L_t \left[\cos^{-1}\left(\frac{L_C}{L_t}\right) - \left(\frac{L_C}{L_t}\right) \sqrt{1 - \left(\frac{L_C}{L_t}\right)^2} \right] \quad (12)$$

where W is

$$\left(\sum_{i=1}^{N_S} \frac{1}{L_i} \right)^{-1}$$

The constant of proportionality in Eq. (12) depends on the conductivity of the tubes. Figure 4 shows a comparison of the analytical result obtained using Eq. (12) with that computed numerically. The ratio q/q_{ref} is plotted, where q_{ref} is the reference heat transfer rate at $L_C/L_t=0.1$. One hundred random realizations of

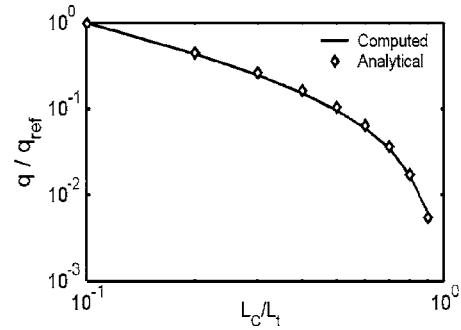


Fig. 4 Comparison of heat transfer rate in a nanotube network with analytical results for the case of zero tube-tube contact

the network for the case $L_C=3 \mu\text{m}$, $H=4 \mu\text{m}$, and $\rho=5.0 \mu\text{m}^{-2}$ are used. The analytical and numerical results are in good agreement with each other, confirming the validity of our approach. When the channel length becomes comparable to or longer than the tube length, q/q_{ref} is seen to go to zero; in the absence of tube-tube and tube-substrate contact, heat, or current can flow through the tubes only if the tubes bridge source and drain. As a practical matter, the result in Fig. 4 is applicable to electrical transport in short-channel CNT/plastic TFTs where the short-channel lengths imply few tube-tube interactions.

Network Conductance Exponent Calculation. Thin film lateral thermal conductivity measurements are generally difficult to perform. Here we compare the network conductance predicted using our model with electrical conductance measurements by Snow et al. [11]. A pure planar tube network is considered, assuming that the substrate is entirely nonconducting. This is typical of electrical transport in CNT/plastic composites. The average length of the tubes in Ref. [11] ranges from 1 to 3 μm . The exact length distribution of nanotubes has not been reported in Ref. [11]. For the numerical model, random networks with a tube length of 2 μm are generated, and an average of over 200 random realizations is taken. The percolation threshold for the network is estimated using $\rho_{\text{th}}=1/\langle L_i \rangle^2$ to be 0.25 μm^{-2} . Simulations are performed for densities in the range 1–10 μm^{-2} for channel lengths varying from 1 to 25 μm^{-2} , and with a width H of 90 μm , corresponding to the dimensionless parameters $L_C/L_t \sim 0.5-12.5$ and $H/L_t=45$. The device dimensions and tube lengths are chosen to match those in Ref. [11].

In Fig. 5(a), the normalized network conductance G/G_0 is shown as a function of L_C/L_t for several tube densities above the percolation threshold for nearly perfect tube-tube contact (i.e., $c_{ij}=50$). For long channels ($L_C > L_t$) there are no tubes directly bridging the source and drain, and current (heat) can flow only because of the presence of the network. If the tube density is greater than the percolation threshold, a continuous path for carrier transport exists from source to drain, and G is seen to be nonzero even for $L_C/L_t > 1$. Figure 5(a) shows that the conductance exponent, n , is close to -1.0 for the high densities ($\rho = 10 \mu\text{m}^{-2}$; $\rho^*=40$), indicating ohmic conduction, in good agreement with Ref. [11]. The exponent increases to -1.80 at lower densities (1.35 μm^{-2} ; $\rho^*=5$), indicating a nonlinear dependence of conductance on channel length. The asymptotic limit of the conductance exponent for infinite samples with perfect tube/tube contact has been found to be -1.97 in Refs. [30,31]. The observed nonlinear behavior for low density is expected because the density value is close to the percolation threshold. Snow et al. reported a conductance-exponent of -1.80 for a density of 1.0 μm^{-2} and channel length $> 5 \mu\text{m}$. For the same device dimensions, this value of the exponent is close to that obtained from our simulations for a density of 1.35 μm^{-2} . At densities close to the percolation threshold, computations are very sensitive to variations in

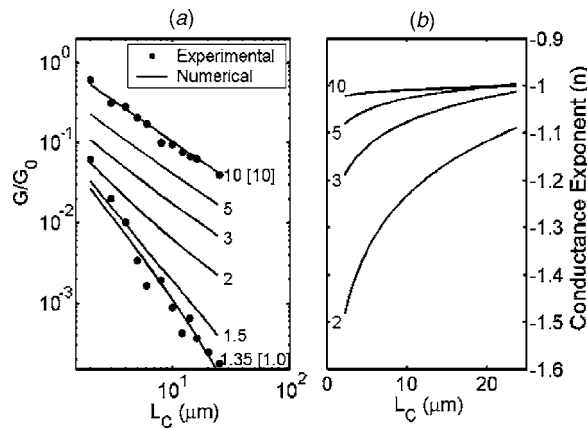


Fig. 5 (a) Computed conductance dependence on channel length for different densities (ρ) in the strong coupling limit ($c_{ij}=50$) compared with experimental results from Ref. [11]. For $\rho=10.0 \mu\text{m}^{-2}$, $G_o=1.0$ (simulation), and $G_o=1.0$ (experiment). For $\rho=1.35 \mu\text{m}^{-2}$, $G_o=1.0$ (simulation) and $G_o=2.50$ (experiment). The number after each curve corresponds to the value of ρ used in the simulation. The number in \square corresponds to ρ in experiments from Ref. [11]; (b) dependence of conductance exponent (n) on channel length for different densities (ρ) based on (a).

computational parameters. Small variations in experimental parameters such as tube diameter, nanotube contact strength, tube electronic properties, as well as the presence of a distribution of tube lengths (1–3 μm), which is not included in the simulation, may explain the difference. The contact resistance between the nanotubes and the source and drain electrodes as well as insufficiently large samples for ensemble averaging in the experimental setup may also be responsible. Some evidence of this is visible in the scatter in the experimental data at low densities.

The dependence of conductance exponent on channel length is explored in Fig. 5(b) for $c_{ij}=50$ and for densities in the range of 2.0–10 μm^{-2} , corresponding to ρ^* values of 8–40. For densities $>3.0 \mu\text{m}^{-2}$ ($\rho^* > 12$), the exponent approaches the ohmic limit, -1.0 , with increasing channel length. Larger exponents, corresponding to nonohmic transport are observed for the shorter channel lengths. This is consistent with experimental observations, where conductance is seen to scale more rapidly with channel length for small L_C [11].

Effective Thermal Conductivity of Nanotube Composites. In this problem, we compute the effective lateral thermal conductivity of a nanotube or nanowire composite. These composites may span a wide range of values of k_s/k_t , Bi_c , and Bi_s . The thermal conductivity of free-standing multiwalled CNTs has been measured at 3000–6000 W/m K [32], though the corresponding values when embedded in a composite are expected to be far smaller due to interface scattering. Though bulk silicon has a thermal conductivity of approximately 150 W/m K at room temperature, the thermal conductivity of Si nanowires in the 22–115-nm-diameter range is one to two orders of magnitude smaller due to phonon boundary scattering and confinement effects [33]. The thermal conductivity of the substrate is generally low, ranging from 0.1 to 1.0 W/m K, leading to a wide range in k_s/k_t . For the present case, we consider values in the 10^{-1} – 10^{-3} range. The values of the tube–tube contact conductance Bi_c and the tube–substrate contact conductance Bi_s are not known. However, our calculations show that $Bi_c > 5$ is tantamount to perfect tube–tube contact. For Bi_s , an estimate of the total thermal resistance between silicon nanowires and a planar interface has been found in Ref. [34] by combining the constriction resistance, gap resistance, and thermal interfacial resistance; however, the model

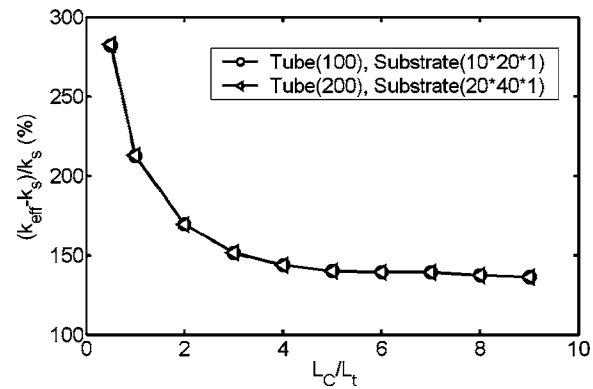


Fig. 6 Increase in composite effective thermal conductivity (k_{eff}) over the substrate value for two different grid sizes: $L_C/L_t=2.0$; $H/L_t=2$, $Bi_c=10.0$, $Bi_s=10^{-5}$, $k_s/k_t=0.001$, and $\rho^*=10.0$

requires the interfacial phonon transmissivity, which must be obtained through experiments or atomistic level simulations. Recent experiments [35] indicate that for CNTs in organic liquids, contact conductance may be extremely low. Yu et al. measured the thermal contact resistance between a carbon fiber and a planar substrate [36]; however, no experimental data are presently available for CNTs or Si NWs embedded in plastic substrates. For the purposes of this simulation, a value of $Bi_s=10^{-5}$ is chosen, consistent with interface resistance values cited in Ref. [35].

Grid independence tests were conducted for the case of $L_C/L_t=2.0$, $H/L_t=2$, $Bi_c=10.0$, $Bi_s=10^{-5}$, $k_s/k_t=0.001$, and $\rho^*=10.0$, corresponding to $L_C=4 \mu\text{m}$, $H=4 \mu\text{m}$, and $\rho=2.5 \mu\text{m}^{-2}$ for non-dimensional channel length L_C/L_t varying from 0.5 to 9 ($L_C=1$ –18 μm). Figure 6 shows the percentage change in the composite thermal conductivity over the substrate value for two different grid sizes. For the first case there are 100 segments per unit tube length, and mesh of $10 \times 20 \times 1$ cells is used in the substrate in the x , y , and z directions, respectively. The second case corresponds to 200 segments per tube, with a mesh of $20 \times 40 \times 1$ cells in the substrate. The results are seen to differ by less than 0.5% between the two cases. The simulations presented in this problem were therefore performed using a mesh of size 100 segments per tube and a mesh of $10 \times 20 \times 1$ cells in the substrate. An average over 200 random realizations is used.

A typical temperature distribution in the tube network and the substrate is shown in Figs. 7(a) and 7(b). For this case, $L_C/L_t=2.0$, $H/L_t=2$, $Bi_c=10.0$, $Bi_s=10^{-5}$, $k_s/k_t=0.001$, and $\rho^*=14.0$, corresponding to $L_C=4 \mu\text{m}$, $L_t=2 \mu\text{m}$, $H=4 \mu\text{m}$, and $\rho=3.5 \mu\text{m}^{-2}$. Contours of constant temperature in the substrate would be one dimensional in x for $Bi_s=0$, but due to the interaction with the tubes, distortion in the contours is observed, consistent with the temperature plots in the tube in Fig. 7(b). The departure from one dimensionality in the substrate temperature profile is related to local variations in tube density; regions of high tube density convey the boundary temperature further into the interior.

The effect of thermal conductivity ratio is explored by varying k_s/k_t from 10^{-1} to 10^{-3} keeping other parameters constant at $L_C/L_t=0.25$ –7.0, $H/L_t=2$, $Bi_c=10.0$, $Bi_s=10^{-5}$, and $\rho^*=10.0$ ($L_C=0.5$ –14 μm , $H=4 \mu\text{m}$, $\rho=2.5 \mu\text{m}^{-2}$). The lower limit would correspond approximately to Si NWs in plastic, accounting for reduced thermal conductivity due to scattering and confinement; the upper limit would correspond approximately to CNTs in plastic. The percentage increase in composite thermal conductivity over that of the substrate is presented in Fig. 8. In general, bulk behavior, whereby the effective thermal conductivity becomes invariant with domain size, is obtained for $L_C/L_t > 5$ or so. Below this, the composite displays finite length effects and is dominated by source–drain bridging for $L_C/L_t < 1$. In general, for bulk

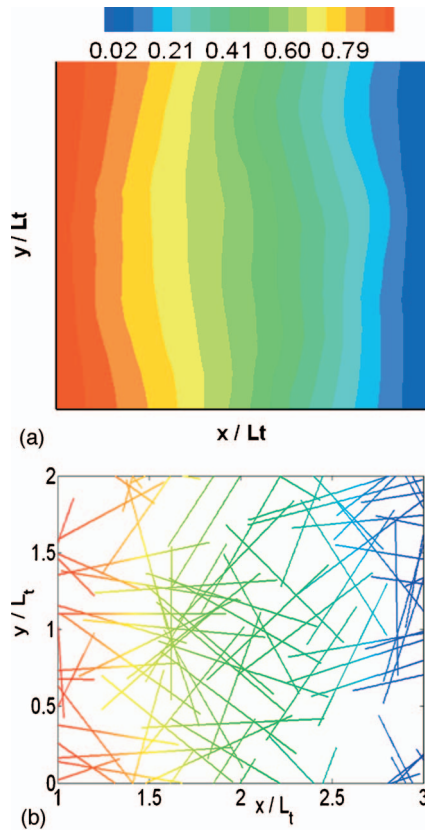


Fig. 7 Nondimensional temperature distribution in (a) substrate (b) tube network: $L_C/L_t=2.0$, $H/L_t=2$, $Bi_c=10.0$, $Bi_s=10^{-5}$, $k_s/k_t=0.001$, and $\rho^*=14.0$

samples, the effective thermal conductivity of the composite may be as much as 125% above k_s for $k_s/k_t=10^{-3}$. However, this only implies a value of k_{eff} in the 0.25–2.5 W/m K, which is still very low, signaling incipient thermal problems in nanocomposite TFTs. As k_s/k_t is increased, some evidence of finite-length effects may still be detected for $k_s/k_t < 5 \times 10^{-3}$. For higher values, though, network conductance ceases to be a dominant contributor and the increase in k_{eff} over k_s drops to zero, signifying that the substrate now dominates conduction through the composite. These computations point to the necessity of accurately characterizing the thermal conductivity of CNTs and Si NWs embedded in substrates. If the presence of the substrate substantially reduces k_t , it is possible that k_s/k_t would be relatively high and the network would no

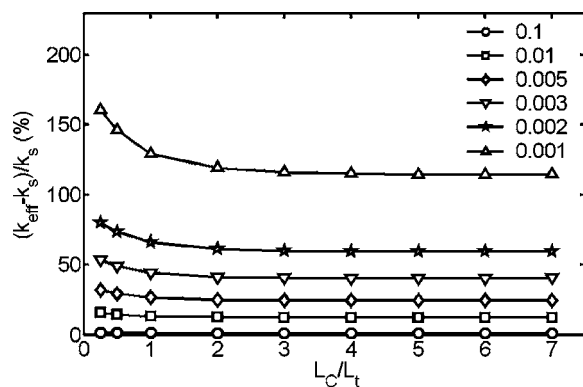


Fig. 8 Effect of substrate-tube conductivity ratio on k_{eff} for varying channel length: $L_C/L_t=0.25-7.0$, $Bi_c=10.0$, $Bi_s=10^{-5}$, and $\rho^*=10.0$

longer provide a significant pathway for heat transfer even if effective tube-tube contact could be maintained. In this limit, in the presence of self-heating, the large surface area of contact between the tubes and the substrate would allow heat to leak from the network to the substrate, and the primary mechanism for heat removal would be the substrate. However, since both substrate and network conductance would be low in this limit, high channel temperatures and degradation of electrical performance may be expected.

Electrical Conductivity of CNT-Organic Composites. The focus of this problem is the prediction of the effective electrical conductivity of CNT-organic composites. Recently, a 60-fold increase in mobility in organic TFTs has been obtained by dispersing high-conducting CNTs in an organic substrate [13]. The carriers flowing from source to drain take advantage of the highly conducting CNT pathways within the semi-conducting organic substrate, flowing partially within the semiconductor and partially through the CNTs. The potential drop across the CNTs is nearly negligible compared to that in the organic substrate, resulting in an overall reduction in the potential drop in the channel for a given drive current. This is equivalent to an effective channel length reduction, or an effective increase in the mobility or electrical conductivity.

The electrical performance of the organic TFT is characterized by the relationship between the drain current I_D and the gate voltage V_G for a given source-drain voltage V_{DS} . The I_D-V_G characteristics of organic TFTs for different volume percent of CNTs has been reported in Ref. [13]. Approximately a third of the CNTs are reported to be metallic, while the rest are semiconducting [13]. Each type has a different electrical conductivity and this heterogeneity must be accounted for in the network model. To reproduce the I_D-V_G curves for this type of device, it is necessary to solve the complete drift-diffusion equations for electrons and holes, in addition to Eq. (6). However, in the linear regime (low V_{DS}) and with $V_G=0$, electrical transport in the organic-CNT composite can be analyzed using Eq. (6). For zero gate voltage, the electrical conductivity of the organic-CNT composite is directly proportional to the current flowing through the TFT. Thus the data in Ref. [13] for $V_G=0$ and low V_{DS} may be used to deduce the effective conductivity of the composite and provide an experimental benchmark against which to test our model.

In order to conduct the computation, it is necessary to determine the density ρ of tubes in the matrix. The CNT fraction in the organic substrate has been reported in terms of volume percent in Ref. [13], while the present model uses a 2D area density ρ to characterize the fraction of CNTs in the substrate. The conversion between the two different representations of the CNT fraction is performed in the following way. It has been reported in Ref. [13] that transistors get shorted at 1% volume fraction of CNT or greater implying that metallic CNTs begin to percolate at this volume fraction. From Ref. [14], the percolation threshold for the CNT network is given by $\rho_{th}=4.236^2/\pi L_s^2=5.7 \mu m^{-2}$ using an average tube length of $1 \mu m$ [13]. Accounting for the fact that one-third of the CNTs are metallic, the total density ρ of the CNTs at 1% volume fraction may be computed as $\rho=3 \times 5.7=17.1 \mu m^{-2}$. Using this conversion, the volume fraction data in Ref. [13] may be converted into the area density ρ needed for our computation.

Device dimensions reported in Ref. [13] are used in the simulation, and correspond to $L_C/L_t=20.0$, $H/L_t=4$, $c_{ij}=10^{-4}$, and $d_{is}=10^{-4}$. The electrical conductivity ratio, σ_t/σ_s , for metallic CNTs is taken as 5.0×10^6 , while that for semiconducting CNTs is 5.0×10^4 [37]. The density ρ is varied in the range 1–17 μm^{-2} , below the percolation threshold. The computed electrical conductivity is presented as a function of dimensionless density ρ^* in Fig. 9. The error bars represent the variability in the prediction for all the realizations computed. The effective electrical conductivity σ_{eff} for both experiments [13] and computations is normalized by

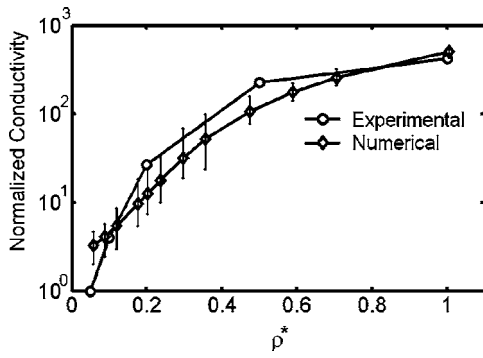


Fig. 9 Comparison of computed conductivity (normalized by the conductivity at $\rho^*=0.05$) of organic transistor against the experimental conductivity [13]

the experimental σ_{eff} at 0.05% volume fraction ($\rho^*=0.05$). Numerical results are found to be in good agreement with the experimental observations over the range of tube densities considered.

Conclusions

In this paper, a computational model for thermal and electrical transport in nanotube composites has been developed and applied to the determination of lateral electrical and thermal conductivity of finite thin films. The model has been verified against analytical solutions, and validated against experimental data for tube densities above and below the percolation threshold, both for nanotube networks in the absence of a substrate, as well as for nanotube-plastic and nanotube-organic composites. Reasonable matches with experimental data have established the general validity of the model.

Nevertheless, a number of important issues remain to be addressed. The model employs thermal contact parameters Bi_c , Bi_s , and electrical contact parameters c_{ij} and d_{is} , which are at present unknown. These must be determined either from careful experiments or from atomistic simulations of tube-tube and tube-substrate contact. Furthermore, while the thermal conductivities of individual freestanding nanotubes and nanowires has been measured and modeled, the modification of these values for tubes and wires encased in plastic or organic substrates is not well understood. Ultimately, our interest is not only in the simulation of conductivity but also in the coupled electro-thermal analysis and design of flexible large-area electronics. Research in these directions is underway and results will be reported in due course.

Acknowledgment

Support of J. Murthy and S. Kumar under NSF Grant Nos. CTS-0312420, CTS-0219098, EE-0228390, the Purdue Research Foundation, and Purdue's Network for Computational Nanotechnology (NCN), is gratefully acknowledged.

Nomenclature

| | |
|----------|--|
| A | = tube cross-sectional area, m^2 |
| A_c | = contact area between tubes, m^2 |
| A_s | = contact area between tube and substrate, m^2 |
| Bi_c | = contact conductance parameter between tubes |
| Bi_s | = contact conductance parameter between tube and substrate |
| c_{ij} | = dimensionless charge-transfer coefficient between tubes |
| d | = diameter of tube, m |
| d_{is} | = dimensionless contact parameter for charge transfer between tube and substrate |
| G | = conductance, Ω^{-1} |

| | |
|---------------------|---|
| h_c | = heat transfer coefficient characterizing tube-tube contact, $\text{W}/\text{m}^2 \text{K}$ |
| h_s | = heat transfer coefficient characterizing tube-substrate contact, $\text{W}/\text{m}^2 \text{K}$ |
| H | = height of the channel, m |
| I_D | = drain current, A/m^2 |
| k_{eff} | = effective lateral thermal conductivity, $\text{W}/\text{m K}$ |
| k_t | = thermal conductivity of tube, $\text{W}/\text{m K}$ |
| k_s | = thermal conductivity of substrate, $\text{W}/\text{m K}$ |
| L_C | = channel length, m |
| L_t | = tube length, m |
| m | = substrate-tube conductivity ratio |
| n | = electron concentration, m^{-3} |
| P_c | = contact perimeter for tube-tube contact, m |
| P_s | = contact perimeter for tube-substrate contact, m |
| s | = length along tube, m |
| t | = substrate thickness, m |
| T | = temperature, K |
| T_i | = temperature of i th tube, K |
| T_s | = substrate temperature, K |
| T_{drain} | = drain temperature, K |
| T_{source} | = source temperature, K |
| v_g | = phonon group velocity, m/s |
| V_G | = gate voltage, V |
| V_{DS} | = drain-source voltage, V |

Greek Symbols

| | |
|---------------------|---|
| θ | = nondimensional temperature |
| ϕ_t | = dimensionless potential distribution along tube |
| ϕ_s | = dimensionless potential distribution in substrate |
| $\Delta \vec{\xi}$ | = displacement vector from tube segment centroid to substrate cell centroid |
| σ | = electrical conductivity, S/m |
| ρ | = tube density, m^{-3} |
| ρ_{th} | = tube density at percolation threshold, m^{-2} |
| ρ^* | = dimensionless tube density ρ/ρ_{th} |
| β_v | = parameter characterizing contact geometry between substrate and tube |
| λ | = mean free path, m |
| τ_r | = phonon residence time in the tube, s |
| τ_b | = time scale for phonon boundary scattering, s |
| $\tau_{3\text{ph}}$ | = time scale for three-phonon scattering processes, s |

Subscripts

| | |
|-------------|---------------------|
| c | = tube-tube contact |
| s | = substrate |
| t | = tube |
| th | = threshold |

Superscript

| | |
|---|------------------|
| * | = nondimensional |
|---|------------------|

References

- [1] Kagan, C. R., and Andry, P., 2003, *Thin Film Transistors*, Marcel-Dekker, New York.
- [2] Madelung, O., ed., 2000, *Technology and Applications of Amorphous Silicon*, Springer, Berlin.
- [3] Dimitrakopoulos, C., and Mascaro, D., 2001, "Organic Thin-film Transistors: A Review of Recent Advances," *IBM J. Res. Dev.*, **45**, pp. 11-27.
- [4] Curioni, A., and Andreoni, W., 2001, "Computer Simulations for Organic Light-Emitting Diodes," *IBM J. Res. Dev.*, **45**, pp. 101-113.
- [5] Wisnieff, R., 1998, "Printing Screens," *Nature (London)*, **394**, pp. 225.
- [6] Pope, M., and Swenberg, C. E., 1999, *Electronic Processes in Organic Crystals and Polymers*, 2nd ed., Oxford University Press, New York, pp. 337-340.
- [7] Peumans, P., 2003, "Small Molecular Weight Organic Thin-Film Photodetectors and Solar Cells," *J. Appl. Phys.*, **93**, pp. 3693-3723.
- [8] Tamura, T., Ogata, K., Takahashi, M., Suzuki, K., Yamaguchi, H., and Todoroki, S., 2000, "Crystal Growth of Laser Annealed Polycrystalline Silicon as a Function of Hydrogen Content of Precursors," *Mater. Res. Soc. Symp. Proc.*, **621**, pp. Q9.5.1-Q9.5.6.
- [9] Ucjikoga, S., 2002, "Low-Temperature Polycrystalline Silicon Thin-Film Tran-

- sistor Technologies for System-on-Glass Displays,” *MRS Bull.*, **27**, pp. 881–886.
- [10] Duan, X., Niu, C., Sahi, V., Chen, J., Parce, J. W., Empedocles, S., and Goldman, J. L., 2003, “High-Performance Thin-Film Transistors Using Semiconductor Nanowires and Nanoribbons,” *Nature (London)*, **425**, pp. 274–278.
- [11] Snow, E. S., Novak, J. P., Campbell, P. M., and Park, D., 2003, “Random Networks of Carbon Nanotubes as an Electronic Material,” *Appl. Phys. Lett.*, **82**(13), pp. 2145–2147.
- [12] Menard, E., Lee, K. J., Khang, D. Y., Nuzzo, R. G., and Rogers, J. A., 2004, “A Printable Form of Silicone for High-Performance Thin-Film Transistors on Plastic Substrates,” *Appl. Phys. Lett.*, **84**(26), pp. 5398–5400.
- [13] Bo, X. Z., Lee, C. Y., Strano, M. S., Goldfinger, M., Nuckolls, C., and Blanchet, G. B., 2005, “Carbon Nanotubes-Semiconductor Networks for Organic Electronics: The Pickup Stick Transistor,” *Appl. Phys. Lett.*, **86**, p. 182102.
- [14] Hu, L., Hecht, D. S., and Gruner, G., 2004, “Percolation in Conducting and Transparent Carbon Nanotube Networks,” *Nano Lett.*, **4**(12), pp. 2513–2517.
- [15] Stauffer, D., and Aharony, A., 1992, *Introduction to Percolation Theory*, 2nd ed., Taylor and Francis, Philadelphia, PA.
- [16] Shenogina, N., Shenogin, S., Xue, L., and Koblinski, P., 2005, “On the Lack of Thermal Percolation in Carbon Nanotube Composites,” *Appl. Phys. Lett.*, **87**, p. 133106.
- [17] Nan, C. W., Liu, G., Lin, Y., and Li, M., 2004, “Interface Effect on Thermal Conductivity of Carbon Nanotube Composites,” *Appl. Phys. Lett.*, **85**(16), pp. 3549–3551.
- [18] Yang, R., and Chen, G., 2004, “Thermal Conductivity Modeling of Periodic Two-Dimensional Nanocomposites,” *Phys. Rev. B*, **69**, p. 195316.
- [19] Milton, G. W., 2002, *The Theory of Composites*, Cambridge University Press, New York.
- [20] Foygel, M., Morris, R. D., Anez, D., Frencs, S., and Sobolev, V. L., 2005, “Theoretical and Computational Studies of Carbon Nanotube Composites and Suspensions: Electrical and Thermal Conductivity,” *Phys. Rev. B*, **71**(10), p. 104201.
- [21] Bieurck, M. J., Liaguno, M. C., Radosavljevic, M., Hyun, J. K., and Johnson, A. T., 2002, “Carbon Nanotubes for Thermal Management,” *Appl. Phys. Lett.*, **80**(15), pp. 2767–2770.
- [22] Liu, C. H., Hunag, H., Wu, Y., and Fan, S. S., 2004, “Thermal Conductivity Improvement of Silicone Elastomer With Carbon Nanotube Loading,” *Appl. Phys. Lett.*, **84**(21), pp. 4248–4250.
- [23] Hasselman, D. P. H., and Johnson, L. F., 1987, “Effective Thermal Conductivity of Composites With Interfacial Barrier Resistance,” *J. Compos. Mater.*, **21**, pp. 508–515.
- [24] Lusti, H. R., and Gusev, A. A., 2004, “Finite Element Predictions for the Thermoelastic Properties of Nanotube Reinforced Polymers,” *Modell. Simul. Mater. Sci. Eng.*, **12**, pp. 107–119.
- [25] Dresselhaus, M. S., and Eklund, P. C., 2000, “Phonons in Carbon Nanotubes,” *Adv. Phys.*, **49**(6), pp. 705–814.
- [26] Kumar, S., Murthy, J. Y., and Alam, M. A., 2005, “Percolating Conduction in Finite Nanotube Networks,” *Phys. Rev. Lett.*, **95**, p. 066802.
- [27] Pierret, R. F., 1996, *Semiconductor Device Fundamentals*, Addison–Wesley, New York.
- [28] Patankar, S. V., 1980, *Numerical Heat Transfer and Fluid Flow*, Hemisphere, New York.
- [29] Kundert, K. S., 1988, *Sparse User’s Guide*, University of California Press, Berkeley, CA.
- [30] Lobb, C. J., and Frank, D. J., 1984, “Percolative Conduction and the Alexander-Orbach Conjecture in Two Dimensions,” *Phys. Rev. B*, **30**(7), pp. 4090–4092.
- [31] Frank, D. J., and Lobb, C. J., 1988, “Highly Efficient Algorithm for Percolative Transport Studies in Two Dimensions,” *Phys. Rev. B*, **37**(1), pp. 302–306.
- [32] Kim, P., Shi, L., Majumdar, A., and McEuen, P. L., 2001, “Thermal Transport Measurements of Individual Multiwalled Nanotubes,” *Phys. Rev. Lett.*, **87**(21), p. 215502.
- [33] Li, D., Wu, Y., Kim, P., Shi, L., Yang, P., and Majumdar, A., 2003, “Thermal Conductivity of Individual Silicon Nanowires,” *Appl. Phys. Lett.*, **83**(14), pp. 2934–2936.
- [34] Prasher, R., 2005, “Predicting the Thermal Resistance of Nanosized Constrictions,” *Nano Lett.*, **5**(11), pp. 2155–2159.
- [35] Huxtable, S. T., Cahill, D. G., Shenogin, S., Xue, L., Oziski, R., Barone, P., Usrey, M., Strano, M. S., Siddons, G., Shim, M., and Koblinski, P., 2003, “Interfacial Heat Flow in Carbon Nanotube Suspensions,” *Nat. Mater.*, **2**, pp. 731–734.
- [36] Yu, C., Saha, S., Zhou, J., Shi, L., Cassell, A. M., Cruden, B. A., Ngo, Q., and Li, J., 2006, “Thermal Contact Resistance and Thermal Conductivity of a Carbon Nanofiber,” *J. Heat Transfer*, **128**, pp. 234–239.
- [37] Seidel, R. V., Graham, A. P., Rajasekharan, B., Unger, E., Liebau, M., Duesberg, G. S., Kreupl, F., and Hoenlein, W., 2004 “Bias Dependence and Electrical Breakdown of Small Diameter Single-Walled Carbon Nanotubes,” *J. Appl. Phys.*, **96**(11), pp. 6694–6699.